Janiszewski, Mateusz; Siren, Topias; Uotinen, Lauri Kalle Tapio; Oosterbaan, Harm; Rinne, Mikael

Effective modelling of borehole solar thermal energy storage systems in high latitudes

Published in:
Geomechanics and Engineering

DOI:
10.12989/gae.2018.16.5.503

Published: 10/12/2018

Document Version
Peer-reviewed accepted author manuscript, also known as Final accepted manuscript or Post-print

Please cite the original version:
Janiszewski, M., Siren, T., Uotinen, L. K. T., Oosterbaan, H., & Rinne, M. (2018). Effective modelling of borehole solar thermal energy storage systems in high latitudes. *Geomechanics and Engineering*, *16*(5), 503-512. https://doi.org/10.12989/gae.2018.16.5.503

Effective Modelling of Borehole Solar Thermal Energy Storage Systems in High Latitudes

Mateusz Janiszewski*[1], Topias Siren[1a], Lauri Uotinen[1b], Harm Oosterbaan[1c] and Mikael Rinne[1d]

[1]*Department of Civil Engineering, School of Engineering. Aalto University, P.O. Box 12100, FI-00076 AALTO, Finland*

(Received keep as blank , Revised keep as blank , Accepted keep as blank)

Abstract. Globally there is an increasing need to reduce the greenhouse gas emissions and increase the use of renewable sources of energy. The storage of solar thermal energy is a crucial aspect for implementing the solar energy for space heating in high latitudes, where solar insolation is high in summer and almost negligible in winter when the domestic heating demand is high. To use the solar heating during winter thermal energy storage is required. In this paper, equations representing the single U-tube heat exchanger are implemented in weak form edge elements in COMSOL Multiphysics® to speed up the calculation process for modelling of a borehole storage layout. Multiple borehole seasonal solar thermal energy storage scenarios are successfully simulated. After 5 years of operation, the most efficient simulated borehole pattern containing 168 borehole heat exchangers recovers 69% of the stored seasonal thermal energy and provides 971 MWh of thermal energy for heating in winter.

Keywords: solar thermal energy, borehole thermal energy storage, numerical modelling, COMSOL, weak form, rock

1. Introduction

Globally there is an increasing need to reduce the greenhouse gas emissions and increase the use of renewable sources of energy. One of the common applications of renewable energy is the solar thermal energy, where energy from the sun is used to heat up water and air in buildings. The seasonal storage of solar thermal energy is a crucial aspect for implementing the solar energy for heating purposes. This is especially important in high latitudes, where the solar insolation is high in the summer but the heating demand is low, and in the winter the situation is reversed.

Thermal energy can be stored underground using several methods. The most common methods include: Aquifer Thermal Energy Storage (ATES), Borehole Thermal Energy Storage (BTES), Tank Thermal Energy Storage (TTES), Pit Thermal Energy Storage (PTES), and Cavern Thermal Energy Storage (CTES), as shown on the conceptual drawing in Figs.1(a)-(e) (Pavlov and Olesen 2012, Novo *et al*. 2010). Thermal energy can also be stored using the so-called HYDROCK method (Fig. 1(f)) that utilises an artificially fractured hard rock aquifer (Larson 1984, Hellström and Larson 2001). The methods can also be combined to enable higher efficiency by using both an underground water tank and boreholes (Reuss *et al*. 2006) or a cavern and boreholes (Nordell *et al*. 1994). Thermal energy can also be stored seasonally in energy piles by using heat exchangers installed in foundations of buildings (Dupray *et al*. 2014, Park and Park 2014). Previously the authors concluded that the BTES is the recommended method for seasonal solar thermal energy storage in crystalline rock environment for a small solar community (Janiszewski *et al*. 2016).

Numerical modelling of borehole heat exchangers (BHE) requires much computational power due to the high ratio of length (over 100 m) and diameter (around 0.1 m) of the borehole. Several approaches exist to model the heat transfer in the BHE. The most elaborate use a fully discretized three-dimensional model with the direct representation of the flow inside the pipes coupled with heat transfer to the surrounding rock mass (e.g. finite volume m0odel by Rees and He, 2013). The advantage of such models is that they can be used to model the thermal behaviour of BHE in very short timescales, where the dynamic variations of the heat transfer are important. However, the fully discretized modelling is memory intensive and time-consuming and not necessary for long-term predictions of seasonal thermal energy storage behaviour.

A more efficient modelling approach with three-dimensional pipe representation is shown by Oberdorfer *et al*. (2011, 2013), where the mean fluid velocity is assumed, and the effective thermal conductivity is calculated based on the average flow velocity and constant parameters (Oberdorfer 2014). Such simplification can reduce the calculation speed and is accurate enough to model the long-term thermal behaviour of one or several borehole heat exchangers.

*Corresponding author, Ph.D. Student,
E-mail: mateusz.janiszewski@aalto.fi
[a]Ph.D., E-mail: topias.siren@rmcf.fi
[b]Ph.D., E-mail: lauri.uotinen@aalto.fi
[c]M.Sc., E-mail: harm.oosterbaan@gmail.com
[d]Ph.D. Professor, E-mail: mikael.rinne@aalto.fi

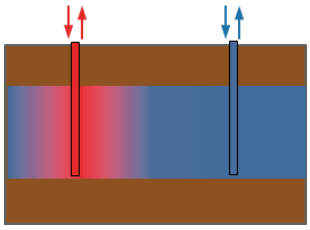

(a) Aquifer Thermal Energy Storage (ATES)

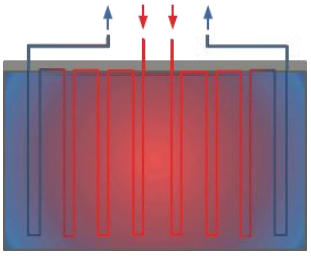

(a) Aquifer Thermal Energy Storage (ATES)

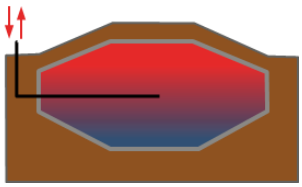

(c) Tank Thermal Energy Storage (TTES)

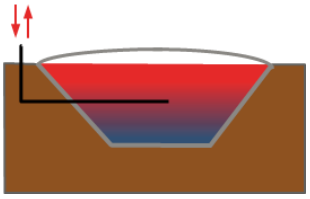

(d) Pit Thermal Energy Storage (PTES)

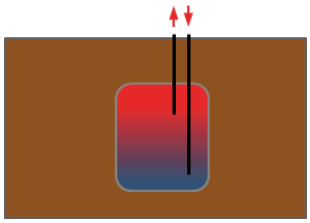

(e) Cavern Thermal Energy Storage (CTES)

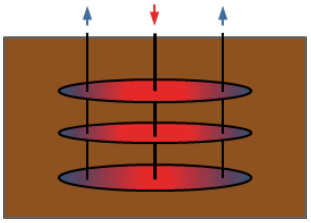

(f) HYDROCK

Fig. 1 Underground thermal energy storage methods

However, BTES facilities may contain an array of over 150 BHEs, and the number of elements required to mesh all BHEs in three-dimensions would be very large, so a faster way of calculating their thermal performance is needed.

A practical approach was first proposed by Al-Khoury *et al*. (2005), where the simplified one-dimensional geometry of BHE is embedded into a three-dimensional medium. While the internal behaviour of a single U-tube borehole heat exchanger can be represented analytically through three equations (Eq. 1–3), it is not possible to solve them directly. However, the solution can be approximated using the weak form equations which interact with the external Finite Element Method (FEM) through shared node points on the BHE edge. This makes the modelling of large borehole fields possible in a relatively short time. Such a simplified approach has been used extensively in the literature (Bauer *et al*. 2011, Diersch *et al*. 2011a, Diersch *et al*. 2011b, Wołoszyn and Gołaś, 2013, Holzbecher and Räuschel, 2014, Ozudogru *et al*. 2014, Welsch *et al*. 2015, Wołoszyn and Gołaś, 2016, Janiszewski *et al*. 2018) as it is appropriate for long-term seasonal storage investigations and results in drastic improvement of calculation speeds, without sacrificing significant accuracy.

In this study, the methodology given by Al-Khoury *et al*. (2005) is implemented by the authors into COMSOL Multiphysics and coupled with heat transfer in the rock mass. This allows fast and efficient simulation of large BTES systems to investigate their long-term performance, and to select the most suitable scenario for a seasonal storage of solar thermal energy in high latitudes.

2. Theoretical framework

The long-term behaviour of an underground thermal storage is studied with 196 days charging period and 168 days discharging period annually. The input temperature is changed using continuous function throughout the year, averaging daily fluctuations out. Therefore, the steady-state heat transfer can be assumed. Eqs. (1)–(3) represent the set of strong form differential equations of the steady-state heat transfer in a single U-tube as given by Al-Khoury *et al*. (2005):

$$-\lambda_r \frac{d^2T_i}{dz^2} dV_i - \rho_r c_r \frac{\alpha u h}{2} \frac{d^2T_i}{dz^2} dV_i + \rho_r c_r u \frac{dT_i}{dz} dV_i + b_{ig}(T_i - T_g) dS_{ig} = 0 \quad (1)$$

$$\lambda_r \frac{d^2T_o}{dz^2} dV_o - \rho_r c_r \frac{\alpha u h}{2} \frac{d^2T_o}{dz^2} dV_o - \rho_r c_r u \frac{dT_o}{dz} dV_o + b_{og}(T_o - T_g) dS_{og} = 0 \quad (2)$$

$$-\lambda_g \frac{d^2T_g}{dz^2} dV_g - \lambda_g \left(\frac{dT_g}{dz} n_z\right) dS_g - b_{ig}(T_g - T_i) dS_{ig} + b_{og}(T_g - T_o) dS_{og} = 0 \quad (3)$$

where the ρ_r is the density and c_r is the heat capacity of the refrigerant fluid. The T_i, T_o, and T_g are the temperatures of the flow-in, flow-out, and grout, respectively. The h is the characteristic length, α is the diffusion term, λ_r and λ_g are the thermal conductivity of the fluid and grout, respectively, and the b_{ig}, and b_{og} are the reciprocals of the thermal resistance between the pipe-in and grout, and pipe-out and grout, respectively.

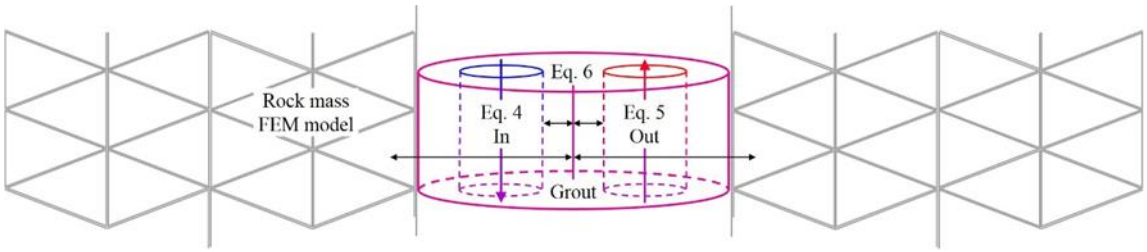

Fig. 2 An illustrative example of the interactions of the implemented heat transfer equations

The strong form equations are converted into a set of weak form equations by multiplying with a test function N^T, integrating by parts, and using the boundary conditions to get Eqs. (4)–(6) after Al-Khoury *et al*. (2005):

$$\int_{V_i} \lambda_r \frac{dN^T}{dz}\frac{dT_i}{dz}dV_i + \int_{V_i} \rho_r c_r u\left(\frac{\alpha h}{2}\frac{dN^T}{dz} + N^T\right)\frac{dT_i}{dz}dV_i + \int_{S_{ig}} b_{ig}N^T\left(T_i - T_g\right)dS_{ig} = 0 \quad (4)$$

$$\int_{V_o} \lambda_r \frac{dN^T}{dz}\frac{dT_o}{dz}dV_o + \int_{V_o} \rho_r c_r u\left(-\frac{\alpha h}{2}\frac{dN^T}{dz} + N^T\right)\frac{dT_o}{dz}dV_o + \int_{S_{og}} b_{og}N^T\left(T_o - T_g\right)dS_{og} = 0 \quad (5)$$

$$\int_{V_g} \lambda_g \frac{dN^T}{dz}\frac{dT_g}{dz}dV_g - \int_{S_g} b_{sg}N^T\left(T_g - T_s\right)dS_g - \int_{S_{ig}} b_{ig}N^T\left(T_g - T_i\right)dS_{ig} - \int_{S_{og}} b_{og}N^T\left(T_g - T_o\right)dS_{og} = 0 \quad (6)$$

where b_{sg} is the reciprocal of the thermal resistance between the grout and surrounding rock. The weak form Eqs. (4)-(6) are then implemented in COMSOL Multiphysics® 5.2a as weak form edge PDEs. The illustrative example of their interactions is shown in Fig. 2.

In Fig. 2, Eqs. (4)-(5) represent the in- and out-going flow temperature at a calculation node, respectively, and Eq. (6) the temperature of the grout that interacts both with the in and out-going flows and the rock mass through FEM mesh.

The heat transport in the rock mass is calculated using the transient heat conduction equation:

$$\rho c\frac{\partial T}{\partial t} + \nabla \cdot -\lambda \nabla T = Q_l \quad (7)$$

where ρ is the density, c is the heat capacity, T is the dependent variable of temperature, and λ is the thermal conductivity of the rock. The Q_l is the line heat source term, which couples Eqs. (6) and (11), representing the heat transfer from the grout into the rock mass:

$$Q_l = b_{sg} \cdot (T_g - T) \cdot S_g \quad (8)$$

The analogy between Fourier's and Ohm's laws for heat flow and current flow is used to find the reciprocals of thermal resistance factors according to the methodology given by Al-Khoury *et al*. (2005). The reciprocals of the thermal resistance between the pipe-in and grout, and pipe-out and grout are equal to each other and are calculated using Eq. (9):

$$b_{ig} = b_{og} = \frac{1}{R_{convection}+R_{pipe}} = \frac{1}{\frac{1}{h_{conv}\cdot\left(\frac{r_o}{r_i}\right)}+\frac{r_o\cdot ln\left(\frac{r_o}{r_i}\right)}{\lambda_p}} \quad (9)$$

where r_o and r_i are the outer and inner radii of the pipes, respectively. The λ_p is the thermal conductivity of the pipe material, and the h_{conv} is the convective heat transfer coefficient assuming turbulent flow conditions inside the pipe and is calculated using Eq. (10):

$$h_{conv} = \frac{Nu\cdot\lambda_r}{2\cdot r_i} = \frac{\left(0.023\cdot Re^{0.8}\cdot Pr^{0.4}\right)\cdot\lambda_r}{2\cdot r_i} = \frac{\left(0.023\cdot\left(\frac{u\cdot 2\cdot r_i}{\nu_r}\right)^{0.8}\cdot\left(\frac{\rho_r \nu_r c_r}{\lambda_r}\right)^{0.4}\right)\cdot\lambda_r}{2\cdot r_i} \quad (10)$$

where Nu is the dimensionless Nusselt number, Re is the Reynolds number, Pr is the Prandtl number, u is the fluid flow velocity, and ν_r is the fluid kinematic viscosity.

The reciprocal of the thermal resistance between the grout and surrounding rock is calculated using Eq. (11):

$$b_{sg} = \frac{1}{2\cdot(R_{convection}+R_{pipe})+R_{grout}} = \frac{1}{2\cdot\left(\frac{1}{h_{conv}\cdot\left(\frac{r_o}{r_i}\right)}+\frac{r_o\cdot ln\left(\frac{r_o}{r_i}\right)}{\lambda_p}\right)+\frac{r_g\cdot ln\left(\frac{r_{eq}}{r_g}\right)}{\lambda_g}} \quad (11)$$

where r_g is the borehole radius, and r_{eq} is the equivalent pipe radius (Eq. (12)) found by creating an equivalent area equal to the sum of the area of both pipes. The equivalent radius is then calculated as:

$$r_{eq} = \sqrt{r_i^2 + r_o^2} \quad (12)$$

The input parameters for the weak form numerical modelling are given in Table 1.

2.1 Comparison with other modelling approaches

The weak form modelling approach (WE) based on Al-Khoury *et al*. (2005) used in this paper is compared with other finite element models to validate the modelling approach and quantify the amount of calculation time that can be saved by using the weak form equations. For this purpose, a single borehole of 10 m length is simulated. The borehole is embedded into a rock cylinder of 5 m radius.

Table 1 Input parameters for the numerical model

	Parameter	Value	Unit	Reference
r_b	Borehole radius	55	mm	Al-Khoury *et al.* (2005)
r_i	Inner pipe radius	16	mm	Al-Khoury *et al.* (2005)
r_o	Outer pipe radius	19	mm	
λ_p	Pipe thermal conductivity	0.3	W/(m·K)	Al-Khoury *et al.* (2005)
λ_s	Ground thermal conductivity	3.2	W/(m·K)	Kukkonen and Peltoniemi (1998)
ρ_s	Ground density	2635	kg/m^3	Kukkonen *et al.* (2011)
c_s	Ground heat capacity	840	J/(kg·K)	Kukkonen and Peltoniemi (1998)
λ_g	Grout thermal conductivity	1.7	W/(m·K)	Chiasson (2016)
λ_r	Fluid thermal conductivity	0.5	W/(m·K)	Al-Khoury *et al.* (2005)
ρ_r	Fluid density	1336	kg/m^3	Al-Khoury *et al.* (2005)
c_r	Fluid heat capacity	2830	J/(kg·K)	Al-Khoury *et al.* (2005)
v_r	Fluid kinematic viscosity	$4.2 \cdot 10^{-6}$	m^2/s	Al-Khoury *et al.* (2005)
u	Fluid flow velocity	0.35	m/s	

The borehole is equipped with a single U-tube BHE and fluid with input properties from Table 1, except the fluid velocity, which is kept constant at 0.6 m/s to ensure turbulent flow conditions inside the pipes. Additionally, the heat capacity of 730 J/kg·K and density of 1680 kg/m^3 is set for the grout material. The pipes have heat capacity equal to 2400 J/kg·K and density equal to 970 kg/m^3. The initial temperature of the rock and the fluid is set to 10 °C. A constant temperature boundary condition of 10 °C is prescribed on the outer and bottom surface of the model. The top surface is made adiabatic. The BHE is charged with a 50°C fluid continuously for 30 days.

First, the BHE is simulated with a Quasi 3D methodology (Q3D) described by Oberdorfer *et al*. (2011), where the BHE geometry is modelled explicitly as a fully three-dimensional object with assumed mean fluid velocity and an effective thermal conductivity of the pipes to calculate the heat transfer through the pipe wall and grout.

Next, the Heat Transfer in Pipes (HTiP) methodology given by Ozudogru *et al*. (2014) is used to simulate the BHE simplified as linear elements that are coupled with the surrounding three-dimensional rock. The so-called pseudo-pipes proposed by the authors are used to account for the heat capacity of pipes.

3. Performance of the weak form modelling approach

The results of the comparison are shown in Fig. 3. The behaviour (shape function) of the fluid temperature is the same for all three models, but the temperature drop of the fluid is different. The two modelling approaches with simplified linear elements (WE and HTiP) predict the highest temperature with the HTiP being lower than WE by 0.26 °C. The Q3D model gives the lowest temperature compared to the other two models (0.53 °C lower than WE). The difference between the models is observed because the weak form assumes a single temperature for the grout, so the grout surrounding the two pipes have the same temperature, even though the two pipes have different temperature. Also, the steady-state formulation of the weak form neglects the heat capacity of the grout. Another explanation is that the linear elements in WE are producing an estimation error due the coupling of grout temperature to the temperature field of the rock mass domains located at the linear element axis and not at the actual outer wall of the grout. The HTiP model introduces a correction approach with “pseudo-pipes” to account for that difference. Hence it gives less error compared to the WE model.

It is also observed that the calculation times are significantly reduced. Although the temperature predicted by the WE model is slightly higher at the outlet compared to other approaches, it takes only 26 s to calculate compared to 518 s for HTiP and 1038 s for Q3D (Fig. 4(a)). The other two methods require much more numerical elements and the number of degrees of freedom solved for (Fig. 4(b)). Also, the virtual memory consumption is much greater as shown in Fig. 4(c).

As long as the behaviour is the same, the weak form modelling can be used for comparison of different scenarios and finding optimum qualitatively and not quantitatively. Hence, the use of WE modelling approach for comparison of large borehole arrays is justified.

4. BTES case study and numerical model set-up

In this paper, the implementation of a weak form edge element is presented with the modelling results of a borehole storage layout using COMSOL Multiphysics® software. The models can be used for the design of the thermal energy borehole storage concept for a small solar community. A set of models was created to study the effects of different storage volumes (20000, 30000, and 40000 m3), height-width (H:W) ratio of the storage (0.5, 1.0, and 3.0) and the number of boreholes connected in series (3 and 6).

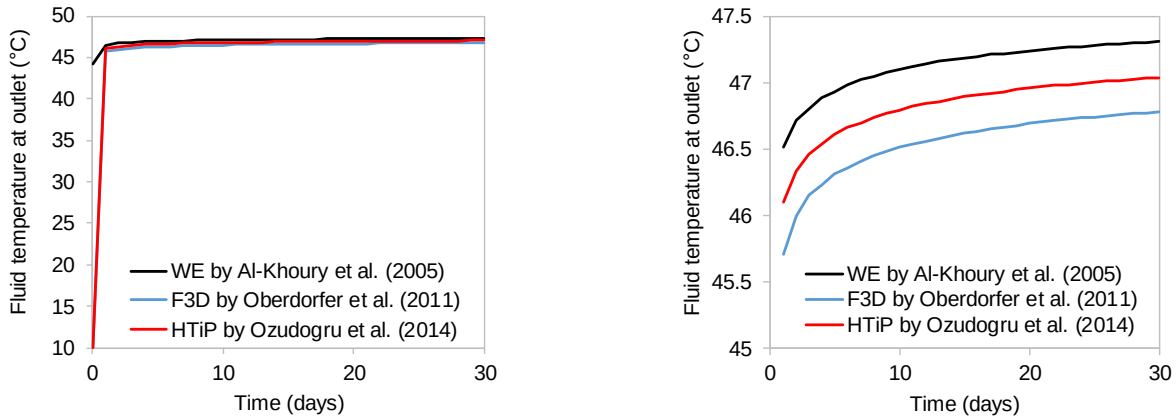

(a) Full time range 0–30 days (b) Data points at day 0 omitted for better visibility

Fig. 3 Comparison of the weak form modelling approach (WE) by Al-Khoury *et al.* (2005) with Quasi 3D (Q3D) numerical model proposed by Oberdorfer *et al.* (2011) and Heat Transfer in Pipes (HTiP) model by Ozudogru *et al.* (2014)

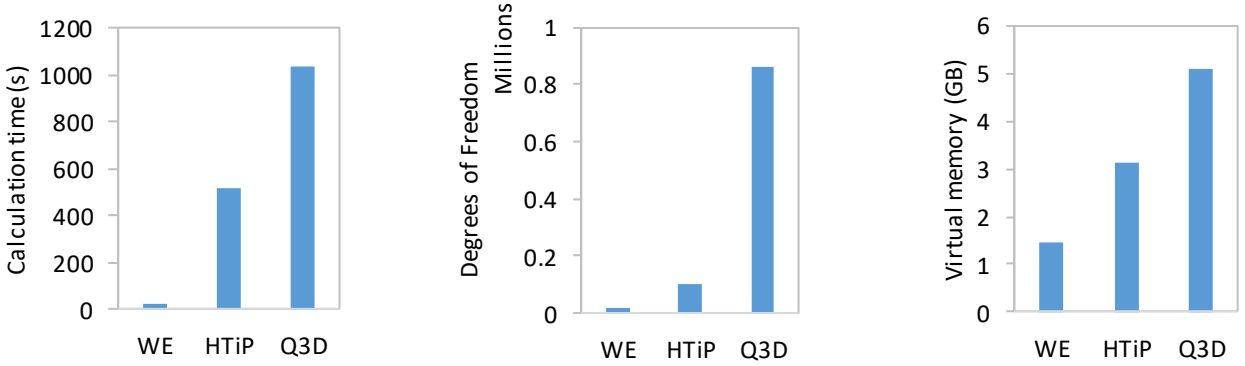

(a) Calculation time (b) Degrees of freedom (c) Virtual memory

Fig. 4 Comparison of the computational requirements of different modelling approaches

The cases with the parameters varied in the study and the resulting borehole metres, the spacing between boreholes, the storage depths, and the diameters are presented in Table 2.

The connectivity of the boreholes is significant for efficient thermal energy storage. Usually, hexagonal borehole pattern is considered as optimal, however, to simplify the modelling a rectangular borehole pattern was used. The two used borehole patterns are illustrated in Figs. 5(a)-(b).

The thermal performance of each scenario is calculated using a quarter symmetric 3D model. In the charging mode, the hot water is inserted from the centre of the borehole field, and it exits at the perimeter. In discharging mode, cold water is injected from the perimeter and exits at the centre.

The amount of charged and discharged energy is calculated based on the following equation:

$$E = \int \Delta T(t) \cdot q \cdot c_r \cdot \rho_r \, dt \tag{13}$$

where ΔT is the temperature difference between the inlet and outlet in each of the BHE loop, q is the volumetric flow rate, c_r is the fluid heat capacity and ρ_r is the fluid density. The energy is summed up for the given amount of BHE loops.

To simplify the model, the average monthly charge/discharge temperatures recorded by Finnish Meteorological Institute (FMI, 2017) are used and the only discharge cycle during the year is used in winter. The assumed charge/discharge temperature function fitted to average outside temperature and taken into account the solar radiation is as follows:

$$T(t) = \sin\left((t + 40)\frac{\pi}{191} - 1\right)30 + 37 \tag{14}$$

where t is the time in days from beginning of the each year cycle on 1st of April (in range from 0 to 364 days). The used borehole field charge/discharge cycle includes 196 days charging period and 168 days discharging period visualised in Fig. 6.

The temperature boundary condition on the top surface and the outer walls follows the sinusoidal surface temperature variation given by Carslaw and Jaeger (1959). The ground temperature varies during the year according to the annual ground surface temperature and attenuates with depth according to the thermal diffusivity of the ground. The temperatures at depth are calculated using Eq. (15):

$$T(z,t) = T_{z,0} + \Delta T_{z,0} e^{-z\cdot\sqrt{\frac{\pi}{P\alpha}}} \cdot \cos\left(\frac{2\pi t}{P} - z \cdot \sqrt{\frac{\pi}{P\alpha}}\right) \tag{15}$$

Table 2 Parameters varied in BTES case study consisting of 18 models in total

Case	No of BHEs	BHEs in series	H:W ratio	Total borehole length, m	Storage volume, m^3	Spacing between boreholes, m	Storage depth, m	Storage diameter, m
48_20000_0.5	48	3	0.5 (wide)	890	20 000	4.6	18.5	37.1
48_20000_1.0	48	3	1.0	1 412	20 000	3.7	29.4	29.4
48_20000_3.0	48	3	3.0 (deep)	2 937	20 000	2.5	61.2	20.4
48_30000_0.5	48	3	0.5	1 018	30 000	4.6	21.2	42.4
48_30000_1.0	48	3	1.0	1 617	30 000	3.7	33.7	33.7
48_30000_3.0	48	3	3.0	3 363	30 000	2.5	70.1	23.4
48_40000_0.5	48	3	0.5	1 121	40 000	5.8	23.4	46.7
48_40000_1.0	48	3	1.0	1 779	40 000	4.6	37.1	37.1
48_40000_3.0	48	3	3.0	3 701	40 000	3.2	77.1	25.7
168_20000_0.5	168	6	0.5	2 854	20 000	2.5	18.5	37.1
168_20000_1.0	168	6	1.0	4 531	20 000	2.0	29.4	29.4
168_20000_3.0	168	6	3.0	9 424	20 000	1.4	61.2	20.4
168_30000_0.5	168	6	0.5	3 267	30 000	2.8	21.2	42.4
168_30000_1.0	168	6	1.0	5 186	30 000	2.2	33.7	33.7
168_30000_3.0	168	6	3.0	10 788	30 000	1.6	70.1	23.4
168_40000_0.5	168	6	0.5	3 596	40 000	3.1	23.4	46.7
168_40000_1.0	168	6	1.0	5 708	40 000	2.5	37.1	37.1
168_40000_3.0	168	6	3.0	11 874	40 000	1.7	77.1	25.7

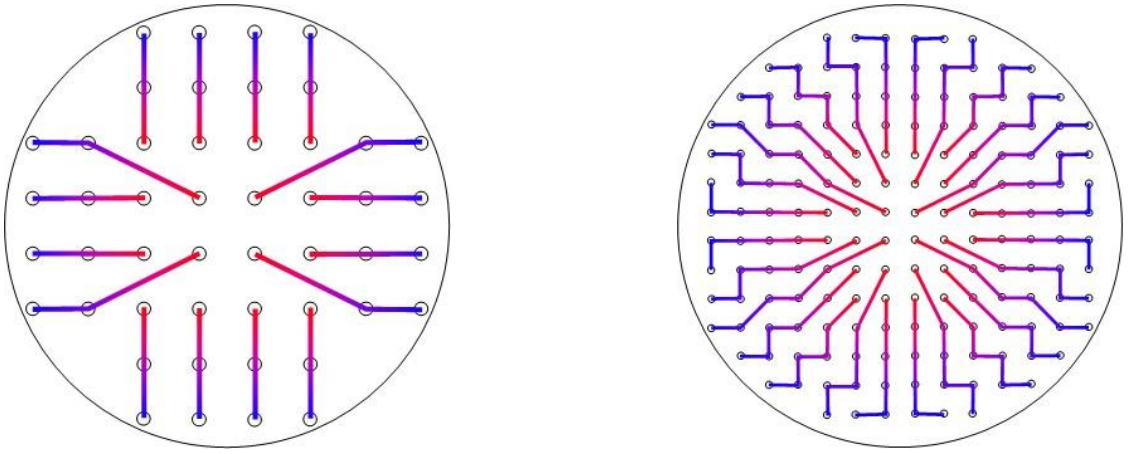

(a) 3 boreholes in series b) 6 boreholes in series

Fig. 5 The two borehole arrays used in the modelling

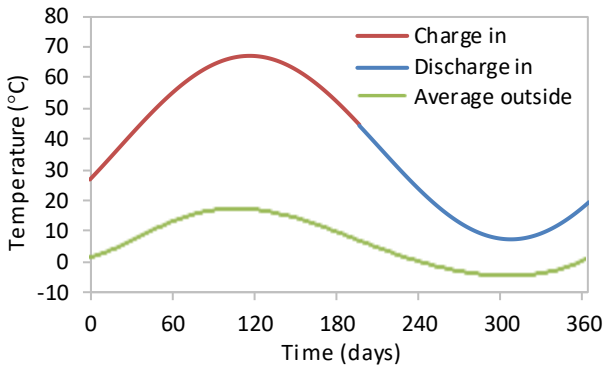

Fig. 6 The charge/discharge and outside temperatures

where $T(z,t)$ is the ground temperature at depth z (calculated from the ground surface) and time t. $T_{z,0}$ is the annual mean ground surface temperature (6.1 °C) calculated from the annual mean surface air temperature using the following relationship $T_{z,0} = 0.71 \cdot T_A + 2.93$ proposed by Kukkonen (1986) to account for the temperature differences of ground and air due to snow cover. The $\Delta T_{z,0}$ is the amplitude of annual ground surface temperatures (8.3 °C), P is the period equal to one year (given in seconds), and α is the thermal diffusivity of the ground. Furthermore, a constant geothermal heat flux h_f equal to 37 mW/m^2 is prescribed on the bottom surface of the model (see Fig. 7). Other input parameters for the model are given in Table 1.

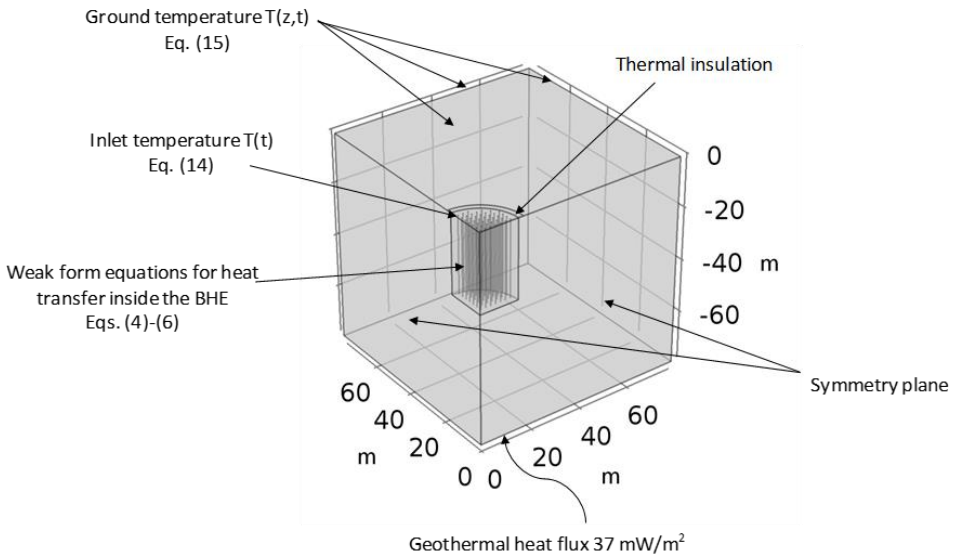

Fig. 7 Description of the boundary conditions in the BTES model

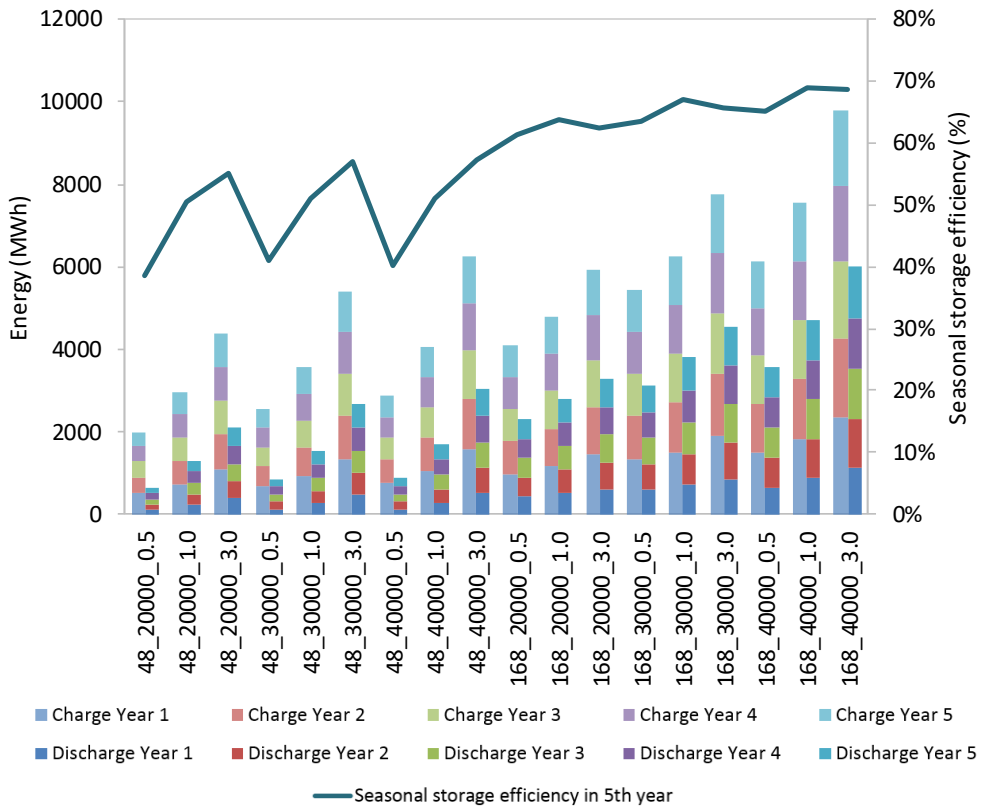

Fig. 8 Comparison of charged and discharged energy during five years of operation, and the seasonal storage efficiency in the 5th year of each scenario

5. Results

The amount of charged and discharged energy in 5 years of operation is presented in Fig. 8. The seasonal storage efficiency is calculated as the ratio of discharged to charged energy. From Fig. 8 it can be seen that the scenarios with 48 boreholes reach a maximum of 57% of seasonal storage efficiency for the storage with 30 000 m^3 volume and 3.0 H:W ratio after 5 years of operation (566 MWh recovered energy). The scenarios with 168 boreholes reach a maximum of 69% of seasonal storage efficiency for the storage with 40 000 m^3 volume and 1.0 H:W ratio after 5 years of operation (971 MWh recovered energy). The increase in the total amount of charged and discharged energy is proportional to the increase in height-to-width (H:W) ratio and the increase in the storage volume. Interestingly, for 48 BHE the 3.0 ratio gives the highest efficiency, but for 168 BHE the 1.0 ratio is more efficient.

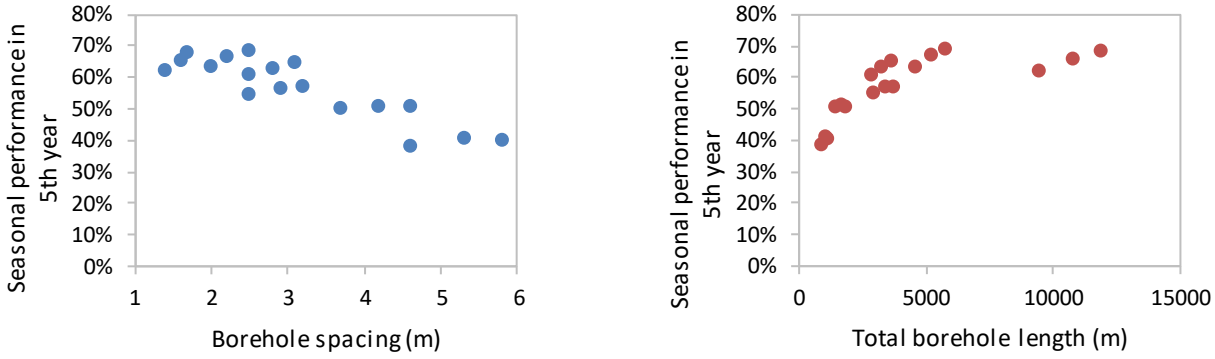

(a) (b)

Fig. 9 The relationship between the seasonal performance in the 5th year to borehole spacing (a) and the total borehole length (b)

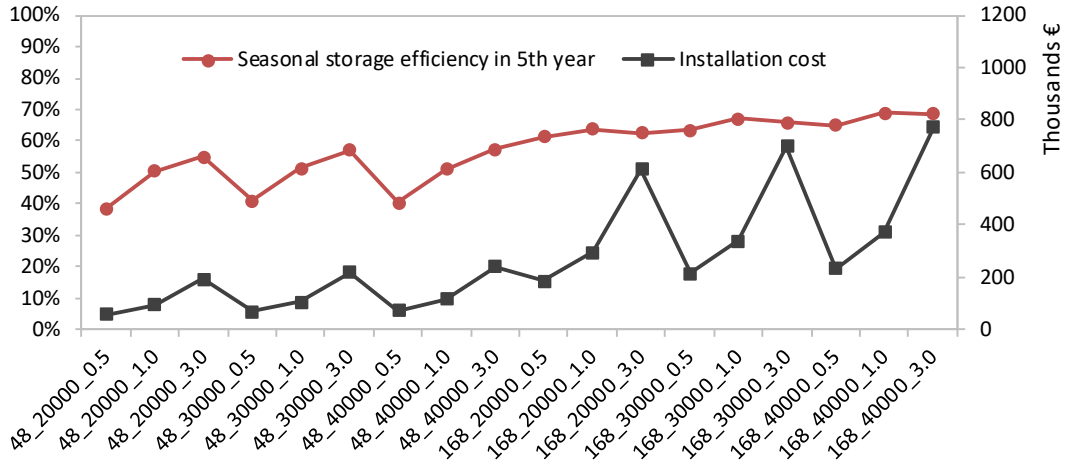

Fig. 10 Comparison of the seasonal storage efficiency and the BHE installation cost of each scenario

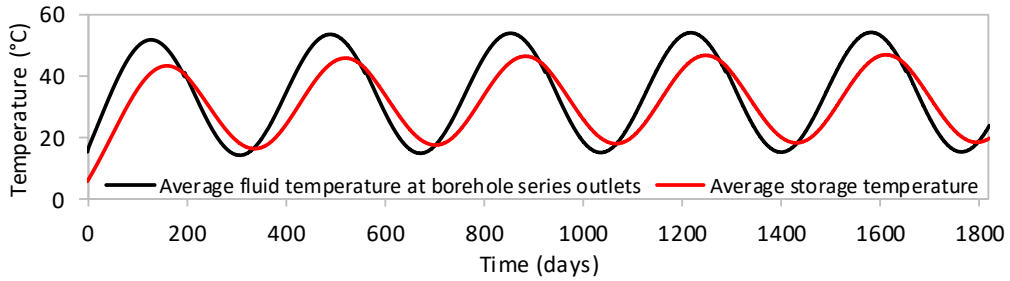

Fig. 11 Average fluid temperatures measured at the series outlets (black) and the average storage temperature (red) of the model with 48 boreholes, 30000 m^3 volume, and 3.0 H:W ratio

Also, the seasonal performance in the 5th year is directly proportional to the total borehole length and inversely proportional to the borehole spacing as shown in Figs. 9(a)-(b). Such result can be explained by the increase in the total length of borehole heat exchangers (as shown in Table 2) as they provide more surface area for heat transfer to take place. It should be noted that the increase in total borehole length will directly influence the installation costs, so the relatively small increase in storage efficiency will result in a drastic increase in the installation cost (Fig. 10).

Assuming an installation cost of 65 €/m (drilling and BHE cost) a 4% increase in the storage efficiency of the most efficient scenario (168_40000_1.0) compared to the scenario with lower H:W ratio (168_40000_0.5) would cost 59% more.

An example of the fluid temperatures measured at the borehole series outlets (on the perimeter in the charging cycle and in the centre in the discharging period) and the average storage temperature is shown in Fig 11. After 5 years the thermal energy storage is balanced, and there is no more increase in the performance.

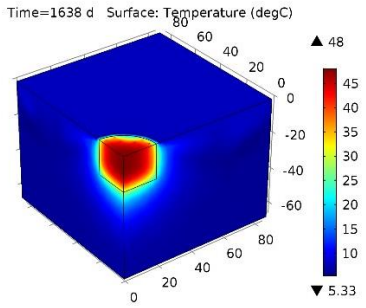

(a) 20000 m^3, H:W ratio 0.5

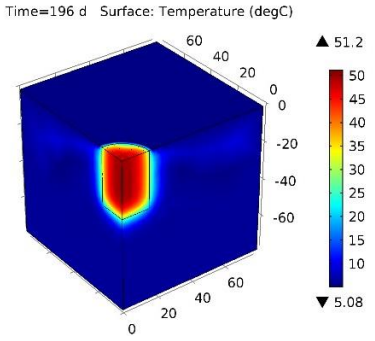

(b) 20000 m^3, H:W ratio 1.5

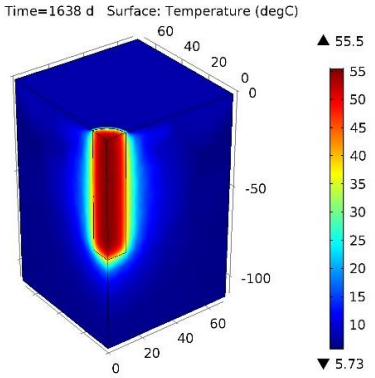

(c) 20000 m^3, H:W ratio 3.0

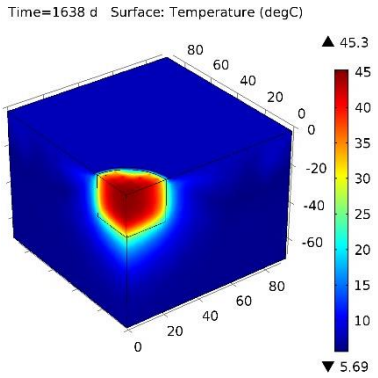

(d) 30000 m^3; H:W ratio 0.5

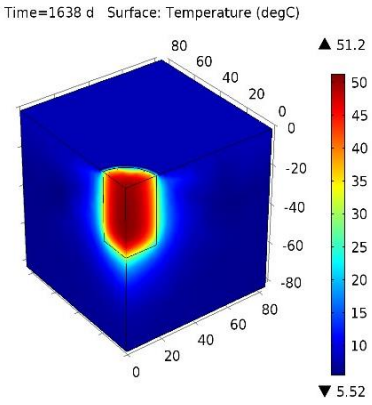

(e) 30000 m^3, H:W ratio 1.0

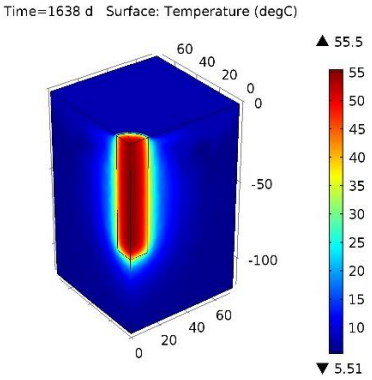

(f) 30000 m^3, H:W ratio 3.0

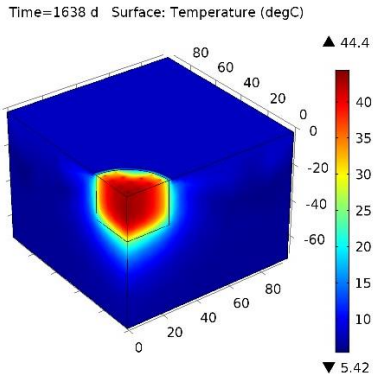

(g) 40000 m^3; H:W ratio 0.5

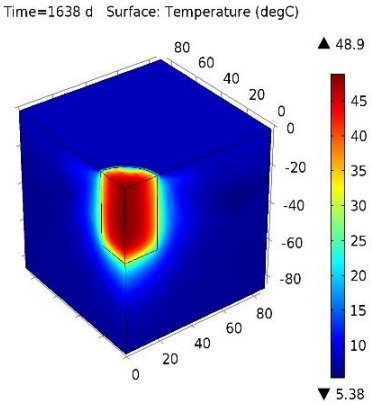

(h) 40000 m^3, H:W ratio 1.0

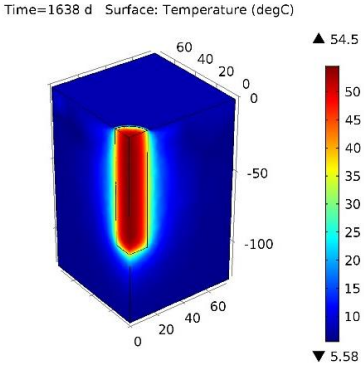

(i) 40000 m^3, H:W ratio 3.0

Fig. 12 Rock temperature of the storage with 48 boreholes after the 5th charging cycle

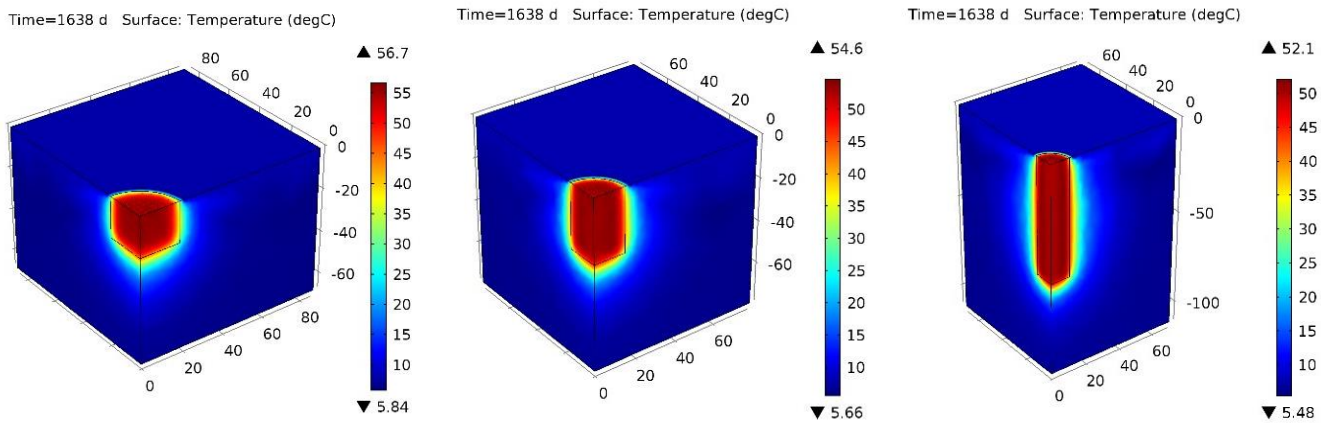

(a) 20000 m^3, H:W ratio 0.5 (b) 20000 m^3, H:W ratio 1.5 (c) 20000 m^3, H:W ratio 3.0

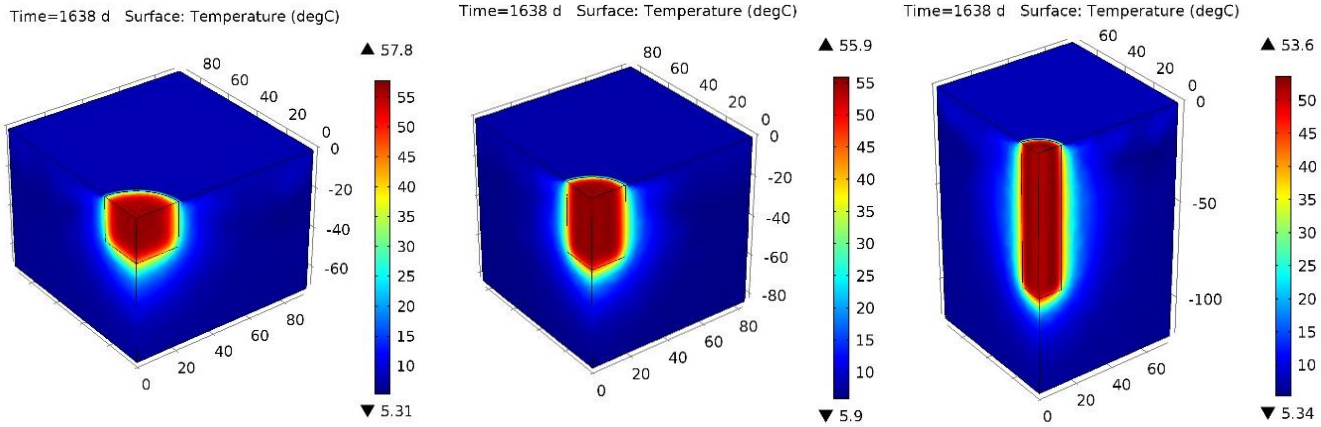

(d) 30000 m^3; H:W ratio 0.5 (e) 30000 m^3, H:W ratio 1.0 (f) 30000 m^3, H:W ratio 3.0

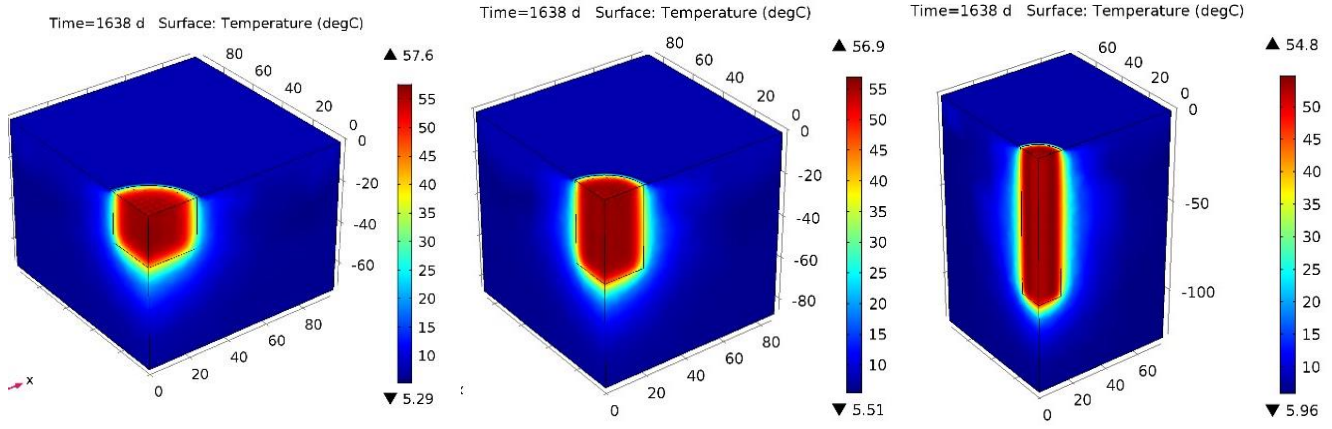

(g) 40000 m^3; H:W ratio 0.5 (h) 40000 m^3, H:W ratio 1.0 (i) 40000 m^3, H:W ratio 3.0

Fig. 13 Rock temperature of the storage with 168 boreholes after the 5th charging cycle

The maximum storage temperature during 5 year modelling period increases up to 55.4 °C for the storage with 48 boreholes (see Figs. 12 (c)-(f)) and up to 57.6 °C for storage with 168 boreholes (see Fig. 13(d)). The bigger the storage volume, the lower the maximum storage temperature, and the more slender shape (high H:W ratio), the higher the maximum temperature.

The maximum relative error of the numerical approximation given by COMSOL is 0.9 % (the last scenario) during the change of the flow direction, caused by the use of steady-state functions. However, the total error is less, as there are only two flow direction changes during

each modelled year. The total calculation time for the five-year simulation using Intel Xeon E3-1230 v5 3.4 GHz processor ranges from 28 min for the first scenario to 9 h 15 min for the last scenario. This confirms that computing the last scenario with other modelling approaches described in section 3 would be extremely demanding, if not impossible.

5. Conclusions

In this study, the thermal performance of seasonal solar thermal energy storage is successfully simulated using the weak form equations of the heat transfer in a single U-tube. The implementation of weak form equations reduces the computing time significantly to reasonable for running multiple calculations of large borehole arrays. The highest performance was achieved with the scenario containing 168 BHEs in 40 000 m^3 storage volume with equal height and width, where 69% of the stored seasonal thermal energy (971 MWh) was recovered after 5 years of operation. However, this scenario costs 59% more than the same scenario with a decreased height-to-width ratio of 0.5, which sacrifices only 4% of the storage efficiency.

The simulations showed that the most efficient storage shape in terms of the seasonal storage efficiency is the height-to-width ratio of 3.0 for the system with 48 BHEs and of 1.0 for the system with 168 BHEs. Also, the seasonal storage efficiency after five years of operation is directly proportional to the total borehole length and inversely proportional to the borehole spacing.

In future research, the weak form approach will be improved by incorporating the specific heat of the grout and improving the thermal resistance network of the borehole heat exchanger by dividing the grout into multiple zones. The transient equations will also be implemented into the weak form edge PDEs to allow better resolution when the flow direction is reversed or the fluid temperature is altered.

Acknowledgments

The funding provided by the Academy of Finland (grant no. 284977) is acknowledged. The help of Aalto University researchers Janne Hirvonen and prof. Jarkko Niiranen is acknowledged.

References

Al-Khoury, R., Bonnier, P.G. and Brinkgreve, R.B.J. (2005), "Efficient finite element formulation for geothermal heating systems. Part I: Steady state", *International Journal for Numerical Methods in Engineering,* **63**(2005), 988–1013.

Bauer, D., Heidemann, W., Muller-Steinhagen, H. and Diersch, H.-J.G. (2011), "Thermal resistance and capacity models for borehole heat exchangers", *Int. J. Energy Res.* **35**(4), 312–320.

Carslaw, H.S. and Jaeger, J.C. (1959), *Conduction of Heat in Solids (2nd Ed.)*, Oxford University Press, Oxford, the UK.

Chiasson, A.D. (2016), "Geothermal Heat Pump and Heat Engine Systems: Theory and Practice", John Wiley & Sons Ltd, Hoboken, NJ, USA.

COMSOL Multiphysics (2017), COMSOL Multiphysics® v. 5.2a., www.comsol.com.

Diersch, H.-J.G., Bauer, D., Heidemann, W., Ruhaak, W. and Schatzl, P. (2011a), "Finite element modeling of borehole heat exchanger systems: Part 1 Fundamentals", *Comput. Geosci.* **37**(8), 1122–1135.

Diersch, H.-J.G., Bauer, D., Heidemann, W., Ruhaak, W. and Schatzl, P. (2011b), "Finite element modeling of borehole heat exchanger systems. Part 2 Numerical simulation", *Comput. Geosci.* **37**(8), 1136–1147.

Dupray, F., Laloui, L. and Kazangba, A. (2014), "Numerical analysis of seasonal heat storage in an energy pile foundation", *Computers and Geotechnics*, **55**(January), 67–77.

FMI (2017), Monthly Statistics, Helsinki, Finland, Finnish Meteorological Institute. http://ilmatieteenlaitos.fi/kuukausitilastot

Hellström, G. and Larson, S. Å. (2001), "Seasonal thermal energy storage - the HYDROCK concept", *Bulletin of Engineering Geology and the Environment,* **60**(2), 145–156.

Holzbecher, E. and Räuschel, H. (2014), Heat transfer in borehole heat exchangers from laminar to turbulent conditions, *Proceedings of the 2014 COMSOL Conference in Cambridge,* Cambridge, UK, February. https://www.comsol.com/paper/download/199569/holzbecher_paper.pdf

Janiszewski, M., Caballero Hernández, E., Siren, T., Uotinen, L., Kukkonen, I. and Rinne, M. (2018), "In Situ Experiment and Numerical Model Validation of a Borehole Heat Exchanger in Shallow Hard Crystalline Rock", *Energies*, **11**(4).

Janiszewski, M., Kopaly, A., Honkonen, M., Kukkonen, I., Uotinen, L., Siren, T. and Rinne, M. (2016), "Feasibility of underground seasonal storage of solar heat in Finland", *International Conference on Geomechanics, Geoenergy and Georesources*, Melbourne, Australia, 959–965.

Kukkonen, I, Peltoniemi, S. (1998), "Relationships between thermal and other petrophysical properties of rocks in Finland", *Phys. Chem. Earth*, **23**(3), 341–349.

Kukkonen, I. (1986), "Menneisyyden ilmastomuutosten vaikutus kallion lämpötilaan ja lämpötilagradienttiin Suomessa (The effect of past climatic changes on bedrock temperature gradients in Finland)", Working report YST-55: Geological Survey of Finland.

Kukkonen, I., Kivekäs, L., Vuoriainen, S., Kääriä, M. (2011), "Thermal properties of rocks in Olkiluoto: results of laboratory measurements 1994–2010", Working report 2011-17, Posiva Oy, Eurajoki, 2011. Available online at: http://www.posiva.fi/files/1504/WR_2011-17_web.pdf

Larson, S.Å. (1984), "Hydraulic fracturing in the Bohus granite, SW-Sweden. Test for heat storage and heat extraction", *Geothermal Resources Council TRANSACTIONS,* **8**, 447–449.

Nordell, B., Ritola, J., Sipilä, K. and Sellberg, B. (1994), "The combi heat store - a combined rock cavern/borehole heat store", *Tunneling and Underground Space Technology*, **9**(2), 243–249.

Novo, A.V., Bayon, J.R., Castro-Fresno, D. and Rodriquez-Hernandez, J. (2010), "Review of seasonal heat storage in large basins: Water tanks and gravel–water pits", *Applied Energy*, **87**(2010), 390–397.

Oberdorfer P., Hu, R., Holzbecher E. and Sauter, M. (2013), "A coupled FEM model for numerical simulation of rechargeable shallow geothermal BHE systems", *Proceedings. Thirty-Eighth Workshop on Geothermal Reservoir Engineering*, Stanford University, Stanford, California, February.

Oberdorfer P., Maier F., and Holzbecher E. (2011), "Comparison of borehole heat exchangers (BHEs): State of the art vs. novel design approaches", *COMSOL Conference 2011*, Milan, Italy.

Oberdorfer, P. (2014), "Heat Transport Phenomena in Shallow Geothermal Boreholes. Development of a Numerical Model and a Novel Extension for the Thermal Response Test Method by

Applying Oscillating Excitations", PhD Dissertation, University of Göttingen, Göttingen, Germany.

Ozudogru, T.Y., Olgun, C.G. and Senol, A. (2014), "3D numerical modeling of vertical geothermal heat exchangers", *Geothermics*, **51**(2014), 312–324.

Park, H. and Park, D. (2014), "Thermal transfer behavior in two types of W-shape ground heat exchangers installed in multilayer soils", *Geomechanics and Engineering. An Int'l Journal*, **6**(1).

Pavlov, G. and Olesen, B. (2012), "Thermal energy storage - A review of concepts and systems for heating and cooling applications in buildings: Part 1—Seasonal storage in the ground", *HVAC&R Research*, **18(**3), 515–538.

Rees, S.J. and He, M. (2013), "A three-dimensional numerical model of borehole heat exchanger heat transfer and fluid flow", *Geothermics*, **46**(2013), 1–13.

Reuss, M., Beuth, W., Schmidt, M. and Schoelkopf, W. (2006), "Solar district heating with seasonal storage in Attenkirchen", *10th International conference on Thermal Energy Storage*, Stockton, USA.

Welsch, B., Rühaak, W., Schulte, D.O., Bär, K., Homuth, S. and Saas, I. (2015), "A comparative study of medium deep borehole thermal energy storage systems using numerical modelling", *Proceedings World Geothermal Congress 2015,* Melbourne, Australia, April.

Wołoszyn, J. and Gołaś, A. (2013), "Modelling of a borehole heat exchanger using a finite element with multiple degrees of freedom", *Geothermics*, **47**(2013), 13–26.

Wołoszyn, J. and Gołaś, A. (2016), "Experimental verification and programming development of a new MDF borehole heat exchanger numerical model", *Geothermics,* **59**(2016), 67–76.